remote sensing

MDPI

Article

Detecting Vegetation to Open Water Transitions in a Subtropical Wetland Landscape from Historical Panchromatic Aerial Photography and Multispectral Satellite Imagery

Lukas M. Lamb [1,*], Daniel Gann [1], Jesse T. Velazquez [1] and Tiffany G. Troxler [2]

[1] Department of Biological Sciences, Florida International University, Miami, FL 33199, USA
[2] Department of Earth and Environment, Florida International University, Miami, FL 33199, USA
* Correspondence: llamb009@fiu.edu; Tel.: +1-305-348-1576

Abstract: Over the last century, direct human modification has been a major driver of coastal wetland degradation, resulting in widespread losses of wetland vegetation and a transition to open water. High-resolution satellite imagery is widely available for monitoring changes in present-day wetlands; however, understanding the rates of wetland vegetation loss over the last century depends on the use of historical panchromatic aerial photographs. In this study, we compared manual image thresholding and an automated machine learning (ML) method in detecting wetland vegetation and open water from historical panchromatic photographs in the Florida Everglades, a subtropical wetland landscape. We compared the same classes delineated in the historical photographs to 2012 multispectral satellite imagery and assessed the accuracy of detecting vegetation loss over a 72 year timescale (1940 to 2012) for a range of minimum mapping units (MMUs). Overall, classification accuracies were >95% across the historical photographs and satellite imagery, regardless of the classification method and MMUs. We detected a 2.3–2.7 ha increase in open water pixels across all change maps (overall accuracies > 95%). Our analysis demonstrated that ML classification methods can be used to delineate wetland vegetation from open water in low-quality, panchromatic aerial photographs and that a combination of images with different resolutions is compatible with change detection. The study also highlights how evaluating a range of MMUs can identify the effect of scale on detection accuracy and change class estimates as well as in determining the most relevant scale of analysis for the process of interest.

Keywords: change detection; historical photograph; supervised classification; land cover; coastal wetlands; Florida Coastal Everglades

Citation: Lamb, L.M.; Gann, D.; Velazquez, J.T.; Troxler, T.G. Detecting Vegetation to Open Water Transitions in a Subtropical Wetland Landscape from Historical Panchromatic Aerial Photography and Multispectral Satellite Imagery. *Remote Sens.* **2022**, *14*, 3976. https://doi.org/10.3390/rs14163976

Academic Editor: Mingming Jia

Received: 20 June 2022
Accepted: 12 August 2022
Published: 16 August 2022

1. Introduction

Coastal wetlands around the world are an economically and ecologically important ecosystem type [1–3]. While only occupying ~15% of global natural wetland area, the ecosystem services provided by coastal wetlands are estimated to have a global monetary value of 20.4 trillion USD/per year [4]. However, coastal wetlands have experienced disproportionately large amounts of degradation, primarily as a result of human-driven land-use change [5,6]. As human activities continue to drive land-use change in coastal wetlands, a key concern is how coastal wetlands will cope with the coupled effect of human activities and 21st century climate change [6].

Climate-change-related drivers of land-cover change in coastal wetlands can broadly be attributed to changes in temperature, precipitation [7–9], and sea-level rise (SLR), with SLR including salinization and increases in inundation [6,10,11]. The impacts of SLR alone present major challenges for coastal wetlands and have the potential to drive significant changes in coastal wetlands due to the disruption of ecogeomorphic feedback loops [11–13]. When ecogeomorphic feedback loops are disrupted because of hydrological shifts imposed by SLR, plant growth may slow down and decrease the stability of the wetland system,

leading to a rapid collapse of plant communities [14–17]. Collapse of plant communities has been well studied in subtropical wetland landscapes, such as the Florida Everglades, and is a key concern of restoration efforts [16,18–20].

Quantifying the conversion of vegetated wetlands to open water is crucial for understanding and estimating the rate and extent of vegetation loss across coastal wetlands [21–23]. Remote sensing offers low-cost methods for monitoring landscape changes across broad spatial and temporal scales, relative to resource-intensive, field-based methods [22,23]. Advances in satellite technology have increased the spatial, temporal, spectral, and radiometric resolution of satellite imagery, which allows for more detailed detection of land-cover changes at very fine scales [23]. This aspect is particularly important for capturing the process of vegetation loss, as the transition of vegetated wetlands to open water occurs at a fine scale and requires a high resolution for early detection.

The advantages of using remote sensing methods to classify and monitor coastal wetlands has long been recognized, with numerous reviews detailing advances in the different aspects of remote sensing applications [21–28]. Initially, reviews focused on the types of sensors available for remote sensing applications in wetlands and their utility in estimating biophysical parameters, such as vegetative biomass, with some discussion of specific classification methods [21,22,24]. By now, a wide range of classification methods exist, with numerous machine learning algorithms having been used for supervised classification of wetland vegetation [28]. Some of the more popular algorithms used for supervised classifications include K-nearest neighbor, maximum likelihood, support vector machines, and random forest [28]. While no single algorithm has been identified as the most optimal for all remote sensing applications, the random forest algorithm has been shown to have a high degree of prediction accuracy when applied to spectral data [29]. The random forest algorithm is a classification tree method that creates an ensemble of trees and combines predictions from each tree to arrive at a single decision tree [30], and it has been used in multiple wetland monitoring studies [28,31–34].

When very high-resolution, modern-day satellite imagery is paired with historical aerial photography, robust analyses of landscape change across long temporal extents can be obtained [22]. Aerial photographs are a valuable tool for assessing land-cover change over time as they pre-date the satellite era (starting in the 1970s) by decades, enabling insight into historic changes in land cover [35]. However, there are numerous challenges involved in the classification of historical photographs, as they are often low-resolution, panchromatic data with limited spectral information and have degraded image quality due to the presence of artifacts in the digitization process that can increase spectral noise [35]. Additionally, historical photographs often lack field reference data from the time of photo acquisition, which limits their use to the differentiation of coarse land-cover classes that can clearly be distinguished. Nonetheless, photographic interpreters can utilize the pattern, texture, shape, size, and color or tone of features, along with experience and knowledge of the region of interest to accurately classify land-cover types [35].

Given the well-documented degradation of wetland ecosystems during the 20th century, the classification of historical photographs and their use in detecting land-cover changes present an opportunity to quantify losses in wetland vegetation across broad spatial and temporal extents. Early uses of historical aerial photographs for change detection in wetlands focused on assessing increases in open water areal extents [36–38]. These studies used differing methods to document transitions from vegetated wetland to open water such as histogram thresholding [22] and manual delineation of wetland boundaries using stereoscopes and planimeters [37,38]. While rudimentary, these early studies recognized the distinct spectral differences between open water and the surrounding vegetation, allowing these two land-cover types to be delineated using image processing techniques [36].

More recently, studies have used a mix of manual delineation, image segmentation, and hierarchical classification to classify historical wetland landscapes [15,39–41]. These studies report highly accurate historical wetland classifications (i.e., >90% overall accuracies), yet they use different methods for quantifying the accuracy and provide no discussion

on why they selected their minimum mapping unit (MMU) or on how the selected MMU affected the detection accuracy. The MMU is defined as "the smallest size area entity to be mapped as a discrete area" [42]. The selection of the MMU affects not only the detection accuracy but also the degree of information loss, as the MMU increases because smaller objects are removed [43,44]. Selecting the MMU size depends on the original image resolution, the characteristics of the landscape (i.e., composition and configuration), and the size of the smallest, discrete feature of interest to be retained [43–45].

Proper selection of an MMU can aid in the accurate detection of open water embedded within a vegetated wetland matrix from panchromatic photography by reducing false positives. False positives can arise due to the variability in brightness values of open water pixels in panchromatic photographs. This variability can be due to (1) mixed pixels, where a pixel may contain a proportion of vegetation and open water, which obscures the open water signal; (2) solar glint reflecting off the water's surface and increasing the brightness values in the photographs; (3) bright spectral noise introduced during the process of scanning the photograph to convert analog data to digital data; (4) misinterpreting dark shadows as water.

Our objectives were three-fold: (1) detect and quantify the transition of vegetated wetland to open water in a coastal wetland landscape over a 72-year period using digital image processing techniques; (2) estimate the accuracy differences for the detection methods when classifying historical panchromatic photographs; (3) determine how the MMU affects the accuracy of open water pond detection in a coastal wetland landscape. To accomplish this, we detected the extent of open water ponds embedded in a coastal graminoid-dominated marsh from very high-resolution 2012 multispectral satellite data. We then assessed how accurately we could detect open water ponds in a historical, panchromatic photograph from 1940, by comparing two classification methods: (1) manual image thresholding and (2) automated classification using the random forest algorithm. We varied the MMU of the 1940 and the 2012 wetland vegetation maps to identify how it affected the accuracy and precision of detecting vegetation transitioning to open water ponds. We evaluated the extent of vegetation to open water transitions across a 72-year period and then quantified the classification accuracy of the 1940 and 2012 wetland classifications and change maps, using a spatially explicit, design-based accuracy assessment (Figure 1). Our goal was to refine methods for combining aerial photographs and multispectral satellite images to assess coastal wetland degradation across multidecadal timescales.

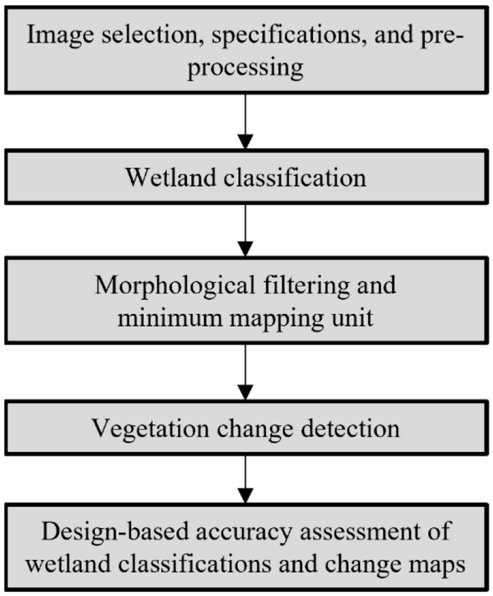

Figure 1. Generalized overview of the wetland classification and change detection methods.

2. Methods

2.1. Study Area

The Florida Everglades, a World Heritage Site, International Biosphere Reserve, and Wetland of International Importance, comprise hundreds of thousands of hectares of marsh, mangrove, and estuarine open water habitat [46]. The southernmost region is home to the Everglades National Park (ENP), where paleoecological studies indicate that some locations are as old as 5700 cal years BP [47] and have seen considerable coastal transgression and regression, indicating the dynamic nature of this coastal environment [48–52]. Since the late 19th century, anthropogenic activities have driven a decrease in hydrologic connectivity between the northern Everglades and the coastal regions [53–55], altering the abiotic conditions necessary for peatland maintenance and growth, leading to a 50% reduction in peat horizontal and vertical extents [55–57].

For this analysis, we focused on a 1.1 × 0.66 km area of coastal marsh along the southwest coast of the ENP for detecting transitions from coastal graminoid marsh to open water pond (Figure 2). The study area was located ~10 km upstream of the Gulf of Mexico, on the south side of the Harney River, a major estuarine channel in ENP (Figure 2). The study area is dominated by two emergent, graminoid marsh species: *Cladium jamaicense* and *Juncus romerianus* (Figure 3A). Vegetative cover of these graminoids can range from high density (100% cover; Figure 3A) to low density (<25% cover; Figure 3B). Interspersed within the graminoid marsh matrix are permanently flooded, unvegetated open water ponds of varying size (Figure 3C) and dense clusters of trees, known as "tree islands", dominated by mangrove and subtropical broad-leaved species (Figure 3A, background).

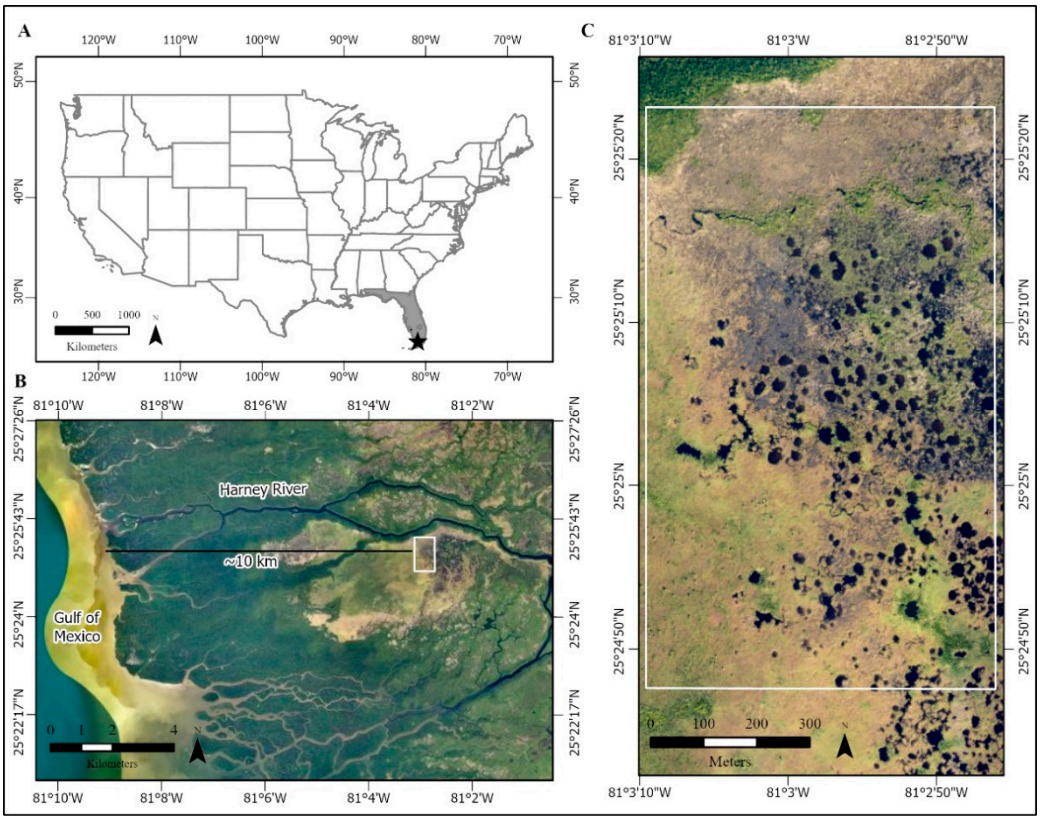

Figure 2. Overview of study area indicating the location of (**A**) the study area (black star) within the state of Florida (grey) in the United States; (**B**) the study area (white rectangle) and its position relative to the southwest coast of Florida with the distance (~10 km) to the Gulf of Mexico indicated; (**C**) the spatial extent (white box) of the study area. The aerial photography used an ArcGIS Pro (v.5.6) imagery base map obtained on 29 January 2021.

Figure 3. Photos from a graminoid dominated marsh in the coastal Everglades showing the major wetland types mapped in this study; (**A**) high-density, graminoid marsh dominated by *Cladium jamaicense* with a tree island dominated by mangrove spp. in the background; (**B**) low-density graminoid marsh interspersed with open water; (**C**) an unvegetated open water pond bordered by *Cladium jamaicense* and the scrub *Rhizophora mangle*.

2.2. Image Selection, Specifications, and Preprocessing

Historical wetland vegetation was mapped from a digitized March 1940 panchromatic aerial photograph. The panchromatic photograph was publicly available and stored in a digital image repository maintained by the United States Geological Survey for the Greater Everglades Ecosystem [58]. The digital copy of the photograph was an 8-bit grayscale panchromatic image, georeferenced to UTM NAD83 zone 17 with a 1 m grid spacing (Foster 2004). Using the *crop* function in the R package *raster* [59], we clipped the photograph to a study area with a maximum east–west extent of 0.66 km and a maximum north–south extent of 1.1 km (Figure 2C). To align the grid spacing of the historical aerial photograph with the high-resolution satellite image, we used bilinear resampling to resample the aerial photograph to the same 2 m grid as the satellite image.

Contemporary vegetation cover was mapped from one, cloud-free, 8-band WorldView-2 (WV-2) satellite image (Digital Globe, Inc., Westminster, CO, USA) obtained on 3 November 2012, which covered the area of the historical photograph. The 2012 WV-2 image was a 16-bit image. The image was geometrically corrected and projected to UTM NAD 83 zone 17 with a 2 m grid spacing using the Rigorous Orthorectification tool in ENVI (v.5.6). Radiometric and atmospheric corrections were also accomplished in ENVI using the radiometric calibration tool to convert digital numbers to radiance. The radiance image was then atmospherically corrected using the Fast Line-of-Sight Atmospheric Analysis of Hypercubes (FLAASH) atmospheric correction module with a mid-latitude summer atmospheric model and maritime aerosol model. A scale factor of 1.0 was set for the bands. Visibility was set at 100 km. The output scale was 10,000 to represent percent reflectance values with 2 decimal precision as integers. Following corrections, the image was clipped to the extent of the study area (Figure 2C) using the *crop* function in the R package *raster* [59].

2.3. Wetland Classification

2.3.1. Classification Scheme

Vegetated wetland generally reflects greater magnitudes of electromagnetic radiation relative to open water bodies, which absorb the majority of incoming solar radiation [36]. This strong spectral separation was observed in both the panchromatic photograph (Figure 4A,C) and the satellite image (Figure 4B,D).

Since the focus of our study was assessing the transition of vegetated wetland to open water, and open water to vegetated wetland, we mapped 1940 and 2012 wetland cover using a binary classification scheme of (1) vegetated wetland and (2) open water. For the 2012 classification, when the reference aerial photography indicated a mixed pixel (see Figure 3B, for example), we assigned a class label of vegetated wetland when the vegetated cover was >50% within the pixel.

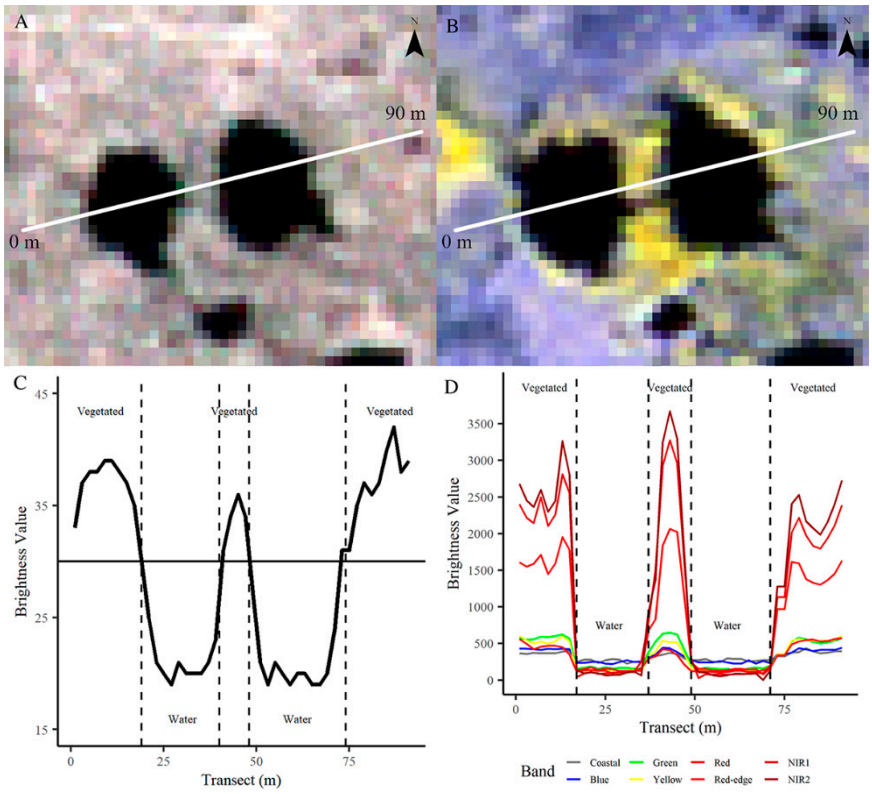

Figure 4. Arbitrary transect across (**A**) the 1940 panchromatic photograph and (**B**) 2012 WorldView-2 image showing the brightness values of the (**C**) panchromatic photograph and the (**D**) WorldView-2 imagery bands.

2.3.2. 1940 Manual Threshold Classification

For the manual threshold classification, visual interpretation of spectral values in the historical photograph determined the threshold value that separated open water from vegetated wetland (Figure 4A,C). Water had very low brightness values relative to the surrounding vegetated wetland, with panchromatic spectral brightness values ranging from 17 to 30 and wetland vegetation > 31 (Figure 4C). Pixels above this brightness value were classified as "vegetated" and below this brightness value as "water".

2.3.3. 1940 and 2012 Automated Machine Learning Classification

For the automated ML classification of the 1940 panchromatic photograph and the 2012 satellite image, we used the random forest algorithm with 5-fold cross-validation using the R package *caret* [60].

For both the 1940 and 2012 random forest classification, we developed training datasets to cover the range of brightness values for each class using on-screen point digitization with samples labeled in ArcGIS Pro (v2.8.0). Characteristics, such as brightness, color, texture, pattern, and context, were used to identify and label samples as either vegetation or open water. For classifying open water in the 1940 photograph, we focused on placing training points within identifiable, discrete open water ponds.

The training datasets totaled 5362 points for the 1940 panchromatic photograph and 5606 points for the 2012 satellite image. The 1940 training dataset had 3082 samples for vegetated wetland and 2280 open water samples, while the 2012 training dataset consisted of 3582 vegetated wetland samples and 2024 open water samples.

For the 1940 training points, brightness values were extracted from the panchromatic photograph. For the 2012 training points, spectral reflectance values of the eight spectral bands and seven vegetation indices were extracted from the satellite image (Table 1). A random forest algorithm was then trained using each dataset. Training datasets were developed using an iterative process where we began with an initial sample of training

points, then added points to locations that were incorrectly classified by the random forest algorithm until the addition of new points did not improve the model's accuracy.

Table 1. WorldView-2 bands and vegetation indices used in the 2012 wetland classification. NIR = near-infrared; RE = red edge.

Band/Vegetation Index	Equation	Reference
Red, Blue, Green, Coastal, Red, NIR1, NRI2, RE	None	N/A
Simple Ratio (SR)	Red/NIR1	[61]
Normalized Difference Vegetation Index (NDVI)	(NIR1 − Red)/(NIR1 + Red)	[62]
Normalized Difference Red-Edge Index (NDRE)	(NIR1 − RE)/(NIR1 + RE)	[63]
Normalized Difference Water Index (NDWI)	(Green-NIR2)/(Green + NIR2)	[64]
Green Normalized Difference Vegetation Index (GNDVI)	(NIR1-Green)/(NIR1 + Green)	[65]
Soil Adjusted Vegetation Index (SAVI)	1.5 × ((NIR1 − Red)/(NIR1 + Red + 0.5))	[66]
Enhanced Vegetation Index (EVI)	2.5 × ((NIR1 − Red)/(NIR1 + 2.4 × Red + 1))	[67]

2.4. Morphological Filtering and Minimum Mapping Unit

Following image classification, we applied a morphological filter to remove vegetation and open water patches smaller than three specified MMUs: 12 m^2 (3 pixels), 24 m^2 (6 pixels), and 36 m^2 (9 pixels). Mathematical morphological frameworks have been used by image analysts for decades as a tool to reduce error rates through an iterative process of dilation (opening) and erosion (closing) operations to remove noisy pixels based on a specified window [68–70]. The morphological filter iteratively filled in patches smaller than the MMU from the edges of the patches to the center, replacing values of those patches with the majority rule applied to a user-defined 3 × 3 kernel size. The morphological filtering algorithm was scripted in R [71]. For the 1940 wetland classification, this resulted in six maps (two classification methods times three MMUs) and for the 2012 wetland classification in three maps (one classification method times three MMUs). We selected the range of MMUs to use 12 m^2 as the smallest MMU to filter single- and two-pixel noise that often occurs due to the vegetation's shadows. The largest MMU we evaluated was 36 m^2, beyond which the loss of open water ponds was considered unacceptable.

Following morphological filtering, we converted each raster-based map to polygons in ArcGIS Pro (v2.8.0) using the Raster to Polygon tool. We then calculated the total count and area of open water ponds to assess how the MMU affected the total number of detected ponds and their size distributions.

2.5. Vegetation Change Detection

To quantify vegetation transitions, we overlaid the filtered wetland maps from 1940 and 2012 and assigned class-change labels to each pixel. The resulting classification had three classes: (1) no change, (2) vegetated wetland to open water, and (3) open water to vegetated wetland. We scripted change detection using R statistical software [71] and assessed per-pixel changes in wetland cover between 1940 and 2012 for each 1940 detection method (n = 2) and each MMU (n = 3), for a total of six change maps.

2.6. Design-Based Accuracy Assessments of 1940 and 2012 Wetland Classifications and Change Maps

We conducted a post-classification design-based accuracy assessment with a stratified random sample design to assess the accuracy of the 1940 and 2012 maps and each change

map. For each accuracy assessment, the spatial assessment unit was the pixel, and agreement was defined as the predicted map label being the same as the reference label. We estimated the sample size needed for each map based on a multinomial distribution with a desired level of confidence of 95% and a precision of 3% [72]. For vegetation maps the number of samples was calculated for the vegetated wetland and open water classes. For the change maps, we sampled the three change classes of no change, vegetated to water, and water to vegetated.

For all accuracy assessments, we sampled a set of reference points for each map (Tables S1 and S2) using the *Strata* function in the R package *sampling* [73]. Samples were visually evaluated and labeled using ArcGIS Pro (v.2.8.0) using the corresponding aerial photograph for each map. Reference points were used to compute an area-based error matrix with adjusted area, adjusted user's accuracy, producer's accuracy, and overall accuracy. We estimated the upper and lower bounds for each accuracy metric with 95% confidence intervals using error matrix reference samples and map ratios [74]. The equations we used for all accuracy estimates can be found in [74].

3. Results

3.1. 1940 Wetland Classification

Across both the thresholding and random forest classifications of the 1940 historical photograph, the overall accuracy and user's accuracy were consistently above 95%, ranging from 96.2 ± 4.8% to 99.8 ± 0.1%, with the MMU only showing a marginal effect on accuracy (Table 2; Figure 5A). For the open water class, the only statistically lower user's accuracy was observed for the random forest classification at an MMU of 24 m^2 (Table 2). The producer's accuracy was consistently above 99% for both classes, except for the threshold classification at an MMU of 24 m^2, which showed a decrease of 50.1 ± 49.2%. The high confidence interval for that accuracy, however, suggests that the estimated accuracy is highly uncertain. The random forest classifier predicted ~50% more open water than the threshold classifier, ranging from 1.9 to 2.2 ha for the random forest classification and from 1.4 to 1.5 ha for the threshold classification.

Table 2. Area-adjusted accuracy estimates (percent ± 95% confidence interval) as well as the total mapped area for wetland classifications for the 1940 panchromatic photograph and 2012 satellite image. Estimates are presented for each 1940 classification method, the 2012 classification, and each minimum mapping unit (MMU). Thres = threshold classifications; rF = random forest classification.

Year and Method	MMU (m^2)	Class	Mapped Area (ha)	Adjusted Area (ha)	Adjusted Producer's Accuracy	Adjusted User's Accuracy	Overall Accuracy
1940 Thres	12	Vegetated	70.4	70.6 ± 0.1	99.8 ± 0.1	100 ± 0.0	99.8 ± 0.1
		Open water	1.5	1.4 ± 0.1	100 ± 0.0	91.5 ± 7.2	
	24	Vegetated	70.5	69.4 ± 2.5	99.7 ± 0.2	96.4 ± 4.9	96.2 ± 4.8
		Open water	1.5	2.6 ± 2.5	50.1 ± 49.2	87.5 ± 8.7	
	36	Vegetated	70.6	70.7 ± 0.1	99.8 ± 0.2	100 ± 0.0	98.8 ± 0.1
		Open water	1.4	1.3 ± 0.1	100 ± 0.0	90.6 ± 0.4	
1940 rF	12	Vegetated	69.8	70.2 ± 0.1	99.7 ± 0.2	100 ± 0.0	99.7 ± 0.1
		Open water	2.2	1.8 ± 0.1	100 ± 0.0	90.4 ± 6.8	
	24	Vegetated	69.9	70.2 ± 0.2	99.5 ± 0.2	100 ± 0.0	99.5 ± 0.2
		Open water	2.0	1.7 ± 0.2	100 ± 0.0	83.1 ± 8.4	
	36	Vegetated	70.0	70.2 ± 0.1	99.7 ± 0.2	100 ± 0.0	99.5 ± 0.2
		Open water	1.9	1.8 ± 0.1	100 ± 0.0	90.4 ± 6.8	

Table 2. *Cont.*

Year and Method	MMU (m^2)	Class	Mapped Area (ha)	Adjusted Area (ha)	Adjusted Producer's Accuracy	Adjusted User's Accuracy	Overall Accuracy
2012 rF	12	Vegetated	68.5	68.1 ± 1.1	99.8 ± 0.1	99.2 ± 1.5	99.1 ± 1.5
		Open water	3.5	3.9 ± 1.1	86.3 ± 23.2	96.8 ± 3.0	
	24	Vegetated	68.6	67.1 ± 1.8	99.8 ± 0.1	97.6 ± 2.7	97.6 ± 2.6
		Open water	3.4	4.9 ± 1.8	66.5 ± 25.0	96.8 ± 3.1	
	36	Vegetated	68.7	68.1 ± 1.1	99.9 ± 0.1	99.1 ± 1.6	99.2 ± 1.5
		Open water	3.3	3.8 ± 1.1	85.1 ± 12.6	99.9 ± 1.6	

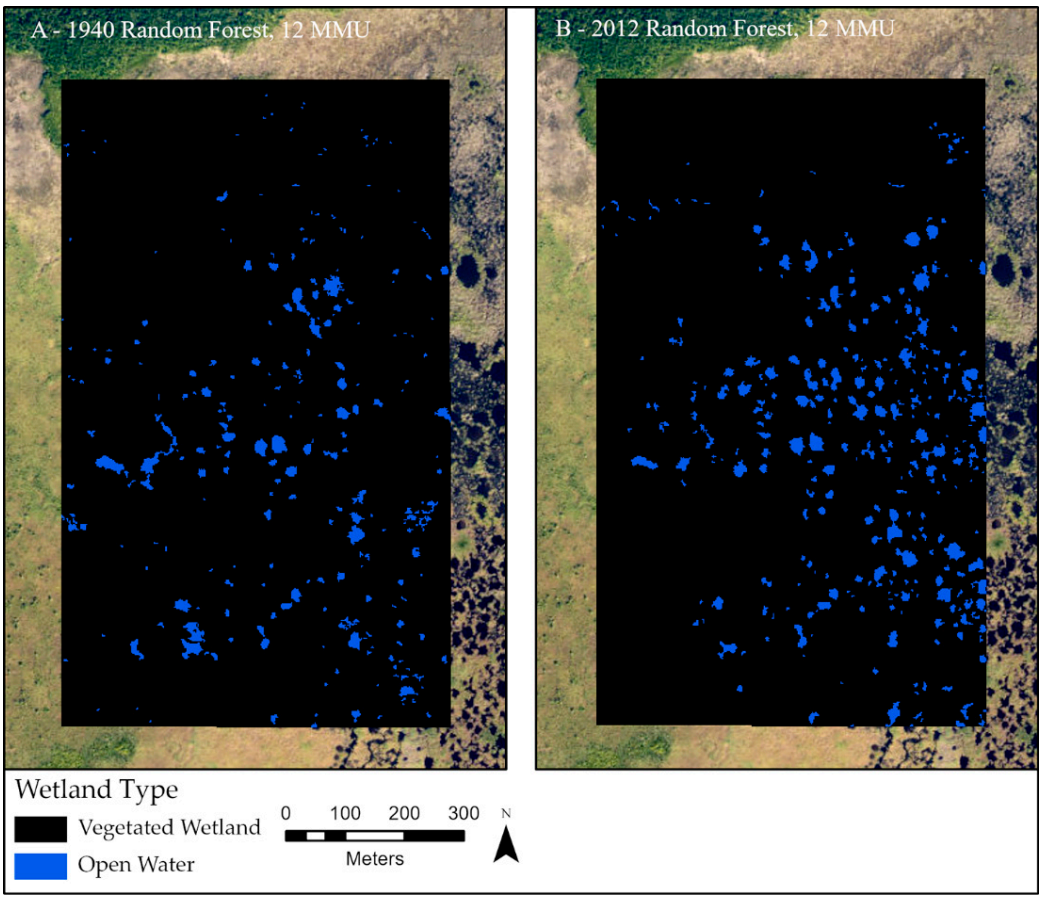

Figure 5. (**A**) 1940 random forest land cover classification; (**B**) 2012 random forest land cover classification. Both classifications are shown at a 12 m^2 MMU.

3.2. 2012 Wetland Classification

For the 2012 random forest wetland land-cover classification, we obtained an overall accuracy and user's accuracy above 96% across all MMU's (Table 2; Figure 5B). The user's accuracy for the vegetated wetland and open water classes were similar across classified wetland maps (Table 2). For the open water class, the producer's accuracy was low, ranging from 66.5 ± 25.0% to 86.3 ± 23.2%.

3.3. Changes in Wetland Classes from 1940 to 2012

Change maps (Figure 6) had overall accuracies above 96%, with the change map comparing the 1940 threshold classification and 2012 classification at a 12 m^2 MMU having the greatest overall accuracy of 99.0 ± 0.3% (Table 3). The highest user's accuracy of

the vegetated wetland to water change class was 83.5 ± 7.2% for the 1940 random forest classification and 2012 classification change map at a 12 m^2 MMU (Table 3). However, the 1940 threshold and 2012 classification at a 24 m^2 MMU had a significantly lower user's accuracy of 70.1 ± 9.7%. This corresponded to a low producer's accuracy for the no-change class, which ranged from 58.9% to 68.3% across all change maps (Table 3). The user's accuracy of the open water to vegetated wetland class was above 50% for all change maps, ranging from 53.2 ± 10.1% to 72.6 ± 9.0%.

The total estimated area of 1940 vegetated wetland that was converted to open water ranged from 2.3 ha (3.2%) to 2.7 ha (3.7%) across all change maps, with a conversion from water to vegetation ranging from 0.6 ha (0.08%) to 1.2 ha (1.7%) across all change map versions (Table 3). The "no-change" class was consistently estimated to have an area of 68.3 ha (94.8%) to 68.7 ha (95.4%) across all change map versions (Table 3).

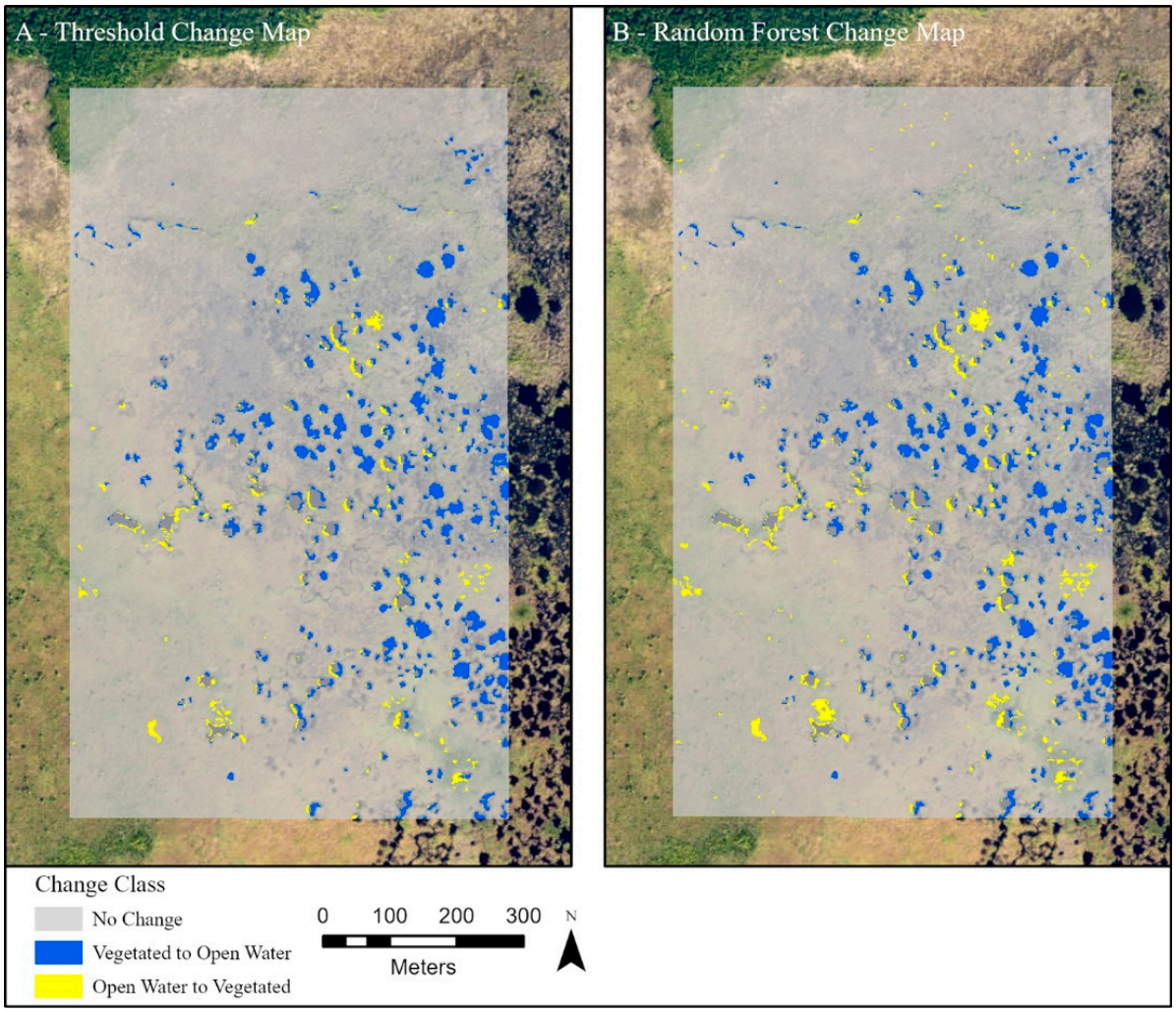

Figure 6. Maps of (**A**) wetland change between the 1940 manual threshold and the 2012 random forest classifications; (**B**) wetland change between the 1940 random forest and 2012 random forest classifications. Both maps are shown at a 12 m^2 MMU. There are three wetland change classes: no change (semitransparent grey), vegetated wetland to open water (blue), and open water to vegetated wetland (yellow).

Table 3. Area-adjusted accuracy estimates for change maps (percent ± 95% confidence interval) including total mapped area. Thres = threshold classifications; rF = random forest classification.

Change Map	MMU (m^2)	Class	Mapped Area (ha)	Adjusted Area (ha)	Adjusted Producer's Accuracy	Adjusted User's Accuracy	Overall Accuracy
1940 Thres, 2012 rF	12	No Change	68.6	69.3 ± 0.2	98.9 ± 0.3	100 ± 0.0	99.0 ± 0.3
		Vegetated to Water	2.7	2.2 ± 0.2	100 ± 0.0	81.1 ± 7.9	
		Water to Vegetated	0.7	0.5 ± 0.1	100 ± 0.0	72.6 ± 9.0	
	24	No Change	68.7	69.5 ± 0.2	98.9 ± 0.3	100 ± 0.0	98.9 ± 0.3
		Vegetated to Water	2.6	2.0 ± 0.2	100 ± 0.0	80.2 ± 8.2	
		Water to Vegetated	0.7	0.4 ± 0.1	100 ± 0.0	63.7 ± 9.9	
	36	No Change	68.9	69.0 ± 1.6	98.6 ± 0.3	98.8 ± 2.2	97.6 ± 2.2
		Vegetated to Water	2.5	2.5 ± 1.6	68.7 ± 42.3	70.1 ± 9.7	
		Water to Vegetated	0.6	0.4 ± 0.1	100 ± 0.0	68.9 ± 9.8	
1940 rF, 2012 rF	12	No Change	68.3	67.9 ± 1.8	98.6 ± 0.3	98.1 ± 2.6	96.9 ± 2.5
		Vegetated to Water	2.5	3.4 ± 1.8	61.1 ± 32.9	83.5 ± 7.2	
		Water to Vegetated	1.2	0.7 ± 0.1	100 ± 0.0	57.3 ± 9.6	
	24	No Change	68.5	68.7 ± 1.4	98.6 ± 0.3	98.9 ± 1.9	98.7 ± 0.3
		Vegetated to Water	2.4	2.0 ± 0.2	100 ± 0.0	81.6 ± 7.7	
		Water to Vegetated	1.1	1.3 ± 1.4	100 ± 0.0	56.1 ± 9.8	
	36	No Change	68.6	68.9 ± 1.4	98.6 ± 0.3	98.9 ± 2.1	97.6 ± 2.0
		Vegetated to Water	2.4	2.5 ± 1.4	71.2 ± 40.2	77.6 ± 8.4	
		Water to Vegetated	1.0	0.5 ± 0.9	100 ± 0.0	53.2 ± 10.1	

3.4. Open Water Pond Detections: Total Count and Size

For the 1940 wetland classification and across the MMUs, the median open water body size was similar across classification methods, but the random forest classification consistently identified more open water bodies than the threshold classification across each MMU (Table 4). For the 2012 wetland classification, the median open water body size increased with the MMU, from 55 m^2 to 97 m^2, while the total number of open water bodies decreased from 307 to 197 (Table 4).

Table 4. Median open water body detection number and median size in square meters (m^2) for 1940 and 2012 wetland maps across classification methods and MMUs of 12, 24, and 36 m^2. Thres = threshold classifications; rF = random forest classification.

Year, Classification-MMU	Total Open Water Body Detections	Median Open Water Area (m^2)
1940, Thres-12	172	43.0
1940, Thres-24	132	58.0
1940, Thres-36	103	80.0
1940, rF-12	251	32.0
1940, rF-24	161	70.0
1940, rF-36	125	87.0
2012, rF-12	307	55.0
2012, rF-24	232	84.5
2012, rF-36	197	97.0

4. Discussion

The results of this study demonstrate that manual thresholding and automated classification methods can achieve similar classification accuracy when classifying wetland landscapes with panchromatic photographs (Table 2). High overall accuracies (>95%) were consistent for all wetland vegetation maps across classification methods and MMUs (Table 2). We obtained high user's and producer's accuracies for vegetated wetland and open water classes; however, in two instances, the producer's accuracy of the open water declined significantly, decreasing to as low as 50.1 ± 49.2%. Further, while change map overall accuracy was consistently above 96%, we obtained multiple change maps with a low user's and/or producer's accuracy, in the range of 50 to 70%. Low class-specific accuracies can be attributed to (1) large differences in proportional class area (Tables S1 and S2) and (2) misclassifications of tree islands in the panchromatic photograph.

4.1. The Importance of Spatially Explicit Accuracy Assessments

Accuracy assessments are critical for quantifying the error and uncertainty of land-cover classifications. The importance of accuracy assessments increases when spatially explicit, detailed, class-specific changes are of interest, rather than just the spatially implicit comparisons of land-cover classes between time points. For point-based accuracy assessments, the number of reference samples per class is determined by the desired confidence and precision level, the proportion of the majority class, and total number of classes [72]. While the proportional area of the majority class was similar across wetland and change maps, the change maps contained three classes while the wetland maps contained two classes (Tables S1 and S2). The increase in class count led to more reference samples per class in the change maps and the identification of misclassified water pixels, and a reduction in the user's and producer's accuracy. Had an implicit estimate of change classes been relied upon, as conducted in other change detection studies [75], we would not have identified these misclassifications. This underscores the need for spatially explicit accuracy assessments of change classes when conducting digital change detection analyses.

When evaluating change classes in a spatially explicit manner, it has also been recommended, and demonstrated here, that estimates of accuracy and areal class cover need to be adjusted for misclassifications that are estimated from the reference dataset. When there are few classes that have large differences in proportional area, small changes in the reference sample error matrix can amount to large changes in estimated accuracy and uncertainty leading to 95% confidence intervals greater than ±40%, as occurred in multiple of our change maps (Table 3). This level of uncertainty makes it impossible to evaluate the producer's accuracy of a map. This demonstrates that even for seemingly trivial remote sensing problems (i.e., differentiating water from vegetation across multidecadal timescales), the methods used to evaluate spatially explicit change need to account for large areal differences in mapped classes and consider adjustments using the error matrix proportions in order to build confidence in the location-specific mapped changes [74].

4.2. Misclassifications and Improving Accuracy

The binary classification scheme of vegetated wetland and open water was predicated on the large difference in spectral reflectance between graminoid marsh and open water in both the panchromatic photograph and high-resolution satellite image (Figure 3). However, in the panchromatic photography, the brightness values of dense clusters of trees were lower and appeared darker than the graminoid vegetation and often resembled grey values of open water areas. The misclassification of tree islands in the 1940 photograph was only apparent when overlaying the photograph on modern-day aerial photographs. This observation required a well-trained aerial photo-interpreter with familiarity of the region, highlighting a challenge of working with historical, panchromatic photographs and the need for developing robust protocols for image processing.

To improve the differentiation of dark pixels, such as open water or tree clusters, additional data sources should be incorporated into the image processing procedure. Tex-

tural analysis has been shown to improve the discrimination of components of vegetation structure in infrared images [76] while also improving the classification accuracy of panchromatic photographs [77,78]. Additionally, stereoscopic imaging can aid in the discrimination of dark pixels that contain vegetation, as stereoscopy allows for a three-dimensional construction of an area and the estimation of vegetation height [79].

4.3. Impact of the Minimum Mapping Unit on Open Water Detection

Across the 72-ha study area, an estimated 2.3 to 2.7 ha of vegetated wetland transitioned to open water across all change map versions (Table 4). This can be attributed to both an increase in the median open water pond size and total count of open water ponds detected (Table 3). Across MMUs, the increases in total open water ponds detected between 1940 and 2012 ranged from 56 to 135 (Table 3), which corresponds to a 22% to 78% increase. The increase in median open water pond size ranged from 12 m^2 to 26.5 m^2. Our images had a spatial resolution of 4 m^2, meaning an MMU of 12 m^2 is a combination of 3 pixels. Based on these results, a 12 m^2 MMU was large enough to filter out noisy pixels but small enough to retain the detail needed to capture the conversion of vegetated wetland to open water. Since conversion of vegetation to open water can occur at spatial scales <1 m^2 in wetland landscapes, such as the Florida Everglades [19], retaining smaller water bodies is desirable and suggests the MMU should be selected at the smallest size possible that still retains high accuracy.

4.4. Ecological Implications

Our finding of losses in vegetation and increases in open water have broader implications for the coastal wetland landscape of the Florida Everglades. In a similar study, manual delineation of historical images was used to assess changes in open water ponds between 1953 and 2009 in the Ten Thousand Islands region of the ENP [16]. The results of this study found a similar increase in total open water ponds and pond size, ranging from 13 m^2 to 31 m^2 across their study area, which had sites that were differentially affected by freshwater management and sea-level rise [16]. Our study area was in a similar ecogeomorphic setting but encompassed a smaller spatial extent and was in a remote setting ~74 km south of [16] and along the southwest coast of the ENP. Both sites have been subjected to hydrologic stresses, but sites within [16] have been more directly impacted by decreased freshwater delivery and saltwater intrusion as a result of the creation of a large canal that intersects their study area [80].

In wetland landscapes, geomorphic processes, such as the collapse of highly organic peat soils, have the potential to drive landscape-level transitions from vegetated wetland to open water [17,81]. A process that can lead to the conversion of vegetated wetland to open water that has recently received considerable attention is "peat collapse" [17,82–84]. Peat collapse is the process of rapid subsidence of the soil surface that alters elevation profiles of the landscape, and it can drive a permanent loss in emergent vegetation, causing a transition to an open water environment [17,85–88]. Across the Florida Everglades, decades of freshwater management has altered the timing, distribution, and volume of freshwater delivery to the coastal estuary and prompted the creation of the largest freshwater restoration effort in the world [20]. There is growing concern that by 2040–2050, the coastal wetland ecosystems will begin a widespread conversion to estuarine conditions [89]. Uncertainty remains at the global scale as to whether coastal wetland spatial extent will increase or decrease over the next century [90], but clearly more regional scale research is needed at broad temporal extents to understand past rates of vegetation loss and better predict their future condition.

5. Conclusions

In this study, a methodology was developed to detect losses in coastal wetland vegetated land cover at the multidecadal scale using a combination of historical panchromatic aerial photography and high-resolution satellite imagery. This methodology was tested

in a coastal peat marsh in the subtropical Florida Everglades, where two methods were compared for classifying historical panchromatic photographs across a range of minimum mapping units to assess the classification accuracy of open water body detection. The results indicate that when classifying historical wetland land cover using panchromatic aerial photography, manual thresholding and automated, machine learning methods can obtain equally accurate classifications in coastal wetland environments, but automated classification methods should be preferentially used if additional data can be obtained that will increase performance. It was also shown how an image analyst's selection of the MMU can impact the classification results, indicating that an MMU should be selected at the smallest size possible, based on spatial resolution and the phenomenon of interest while delivering high-accuracy maps that allow for location-specific analysis of landscape-scale processes such as peat collapse. Further, the importance of conducting point-based accuracy assessments on change maps when performing digital change detection analyses was also underscored, as misclassifications can go undetected in classification map accuracy assessments, and this error will propagate to the change maps. Including the confusion matrix in accuracy assessments assists in the evaluation of uncertainty and areal cover estimation, even when the overall accuracy of the maps is high. This methodology can be applied across broad spatial extents in order to assess degradation and vegetation loss in coastal wetland environments that may have occurred over the last century due to the fact of anthropogenic- and climate-related impacts in order to better predict an uncertain future.

Supplementary Materials: The following supporting information can be downloaded at: https://www.mdpi.com/article/10.3390/rs14163976/s1, Table S1: classified wetland maps accuracy assessment; Table S2: Change maps accuracy assessment; Figure S1: Frequency distribution of open water pond sizes for each 1940 and 2012 classification across minimum mapping units.

Author Contributions: Conceptualization, L.M.L., D.G. and T.G.T.; methodology, L.M.L. and D.G.; formal analysis, L.M.L., J.T.V. and D.G.; original draft preparation, L.M.L. and D.G.; writing—review and editing, L.M.L., D.G., J.T.V. and T.G.T.; visualization, L.M.L.; supervision, T.G.T. All authors have read and agreed to the published version of the manuscript.

Funding: L.M.L. and J.T.V. are grateful for support through the Everglades Foundation FIU ForEverglades Scholarship. L.M.L. was additionally supported by Florida Sea Grant (R/C-S-86), with the collaborative cooperation and financial support of the South Florida Water Management District, and the National Park Service. L.M.L. was also supported by the National Science Foundation award (DBI-1237517), to the Florida Coastal Everglades Long-Term Ecological Research (FCE-LTER) program.

Data Availability Statement: Scripts for the R code, classification maps, change maps, and accuracy assessments will be made publicly available via the Environmental Data Initiative data repository and stored in the Florida Coastal Everglades Long-Term Ecological Research data archive upon publication.

Acknowledgments: The authors thank Jennifer Richards and three anonymous reviewers for their insightful comments. This is contribution #1469 from the Institute of Environment at Florida International University.

Conflicts of Interest: The authors declare no conflict of interest.

References

1. Barbier, E.B.; Hacker, S.D.; Kennedy, C.; Koch, E.W.; Stier, A.C.; Silliman, B.R. The value of estuarine and coastal ecosystem services. *Ecol. Monogr.* **2011**, *81*, 169–193. [CrossRef]
2. Mitsch, W.J.; Gosselink, J.G. *Wetlands*; John Wiley & Sons: New York, NY, USA, 2015; p. 752.
3. Davidson, N.C.; Fluet-Chouinard, E.; Finlayson, C.M. Global extent and distribution of wetlands: Trends and issues. *Mar. Freshw. Res.* **2018**, *69*, 620–627. [CrossRef]
4. Davidson, N.; Van Dam, A.; Finlayson, C.; McInnes, R. Worth of wetlands: Revised global monetary values of coastal and inland wetland ecosystem services. *Mar. Freshw. Res.* **2019**, *70*, 1189–1194. [CrossRef]
5. Mcleod, E.; Chmura, G.L.; Bouillon, S.; Salm, R.; Björk, M.; Duarte, C.M.; Lovelock, C.E.; Schlesinger, W.H.; Silliman, B.R. A blueprint for blue carbon: Toward an improved understanding of the role of vegetated coastal habitats in sequestering CO_2. *Front. Ecol. Environ.* **2011**, *9*, 552–560. [CrossRef]

6. Kirwan, M.L.; Megonigal, J.P. Tidal wetland stability in the face of human impacts and sea-level rise. *Nature* **2013**, *504*, 53–60. [CrossRef] [PubMed]
7. Osland, M.J.; Enwright, N.M.; Day, R.H.; Gabler, C.A.; Stagg, C.L.; Grace, J.B. Beyond just sea-level rise: Considering macroclimatic drivers within coastal wetland vulnerability assessments to climate change. *Glob. Change Biol.* **2016**, *22*, 1–11. [CrossRef]
8. Osland, M.J.; Gabler, C.A.; Grace, J.B.; Day, R.H.; McCoy, M.L.; McLeod, J.L.; From, A.S.; Enwright, N.M.; Feher, L.C.; Stagg, C.L. Climate and plant controls on soil organic matter in coastal wetlands. *Glob. Change Biol.* **2018**, *24*, 5361–5379. [CrossRef]
9. Osland, M.J.; Grace, J.B.; Guntenspergen, G.R.; Thorne, K.M.; Carr, J.A.; Feher, L.C. Climatic controls on the distribution of foundation plant species in coastal wetlands of the conterminous United States: Knowledge gaps and emerging research needs. *Estuaries Coasts* **2019**, *42*, 1991–2003. [CrossRef]
10. Herbert, E.R.; Boon, P.; Burgin, A.J.; Neubauer, S.C.; Franklin, R.B.; Ardón, M.; Hopfensperger, K.N.; Lamers, L.P.; Gell, P. A global perspective on wetland salinization: Ecological consequences of a growing threat to freshwater wetlands. *Ecosphere* **2015**, *6*, 1–43. [CrossRef]
11. Cahoon, D.R.; McKee, K.L.; Morris, J.T. How Plants Influence Resilience of Salt Marsh and Mangrove Wetlands to Sea-Level Rise. *Estuaries Coasts* **2020**, *44*, 883–898. [CrossRef]
12. Cahoon, D.R.; Hensel, P.F.; Spencer, T.; Reed, D.J.; McKee, K.L.; Saintilan, N. Coastal wetland vulnerability to relative sea-level rise: Wetland elevation trends and process controls. In *Wetlands and Natural Resource Management*; Springer: Berlin/Heidelberg, Germany, 2006; pp. 271–292.
13. Day, J.W.; Christian, R.R.; Boesch, D.M.; Yáñez-Arancibia, A.; Morris, J.; Twilley, R.R.; Naylor, L.; Schaffner, L. Consequences of climate change on the ecogeomorphology of coastal wetlands. *Estuaries Coasts* **2008**, *31*, 477–491. [CrossRef]
14. Morris, J.T.; Sundareshwar, P.; Nietch, C.T.; Kjerfve, B.; Cahoon, D.R. Responses of coastal wetlands to rising sea level. *Ecology* **2002**, *83*, 2869–2877. [CrossRef]
15. Schepers, L.; Kirwan, M.; Guntenspergen, G.; Temmerman, S. Spatio-temporal development of vegetation die-off in a submerging coastal marsh. *Limnol. Oceanogr.* **2017**, *62*, 137–150. [CrossRef]
16. Andres, K.; Savarese, M.; Bovard, B.; Parsons, M. Coastal wetland geomorphic and vegetative change: Effects of Sea-level rise and water management on brackish marshes. *Estuaries Coasts* **2019**, *42*, 1308–1327. [CrossRef]
17. Chambers, L.G.; Steinmuller, H.E.; Breithaupt, J.L. Toward a mechanistic understanding of "peat collapse" and its potential contribution to coastal wetland loss. *Ecology* **2019**, *100*, e02720. [CrossRef]
18. Wilson, B.J.; Servais, S.; Charles, S.P.; Davis, S.E.; Gaiser, E.E.; Kominoski, J.S.; Richards, J.H.; Troxler, T.G. Declines in plant productivity drive carbon loss from brackish coastal wetland mesocosms exposed to saltwater intrusion. *Estuaries Coasts* **2018**, *41*, 2147–2158. [CrossRef]
19. Charles, S.P.; Kominoski, J.S.; Troxler, T.G.; Gaiser, E.E.; Servais, S.; Wilson, B.J.; Davis, S.E.; Sklar, F.H.; Coronado-Molina, C.; Madden, C.J. Experimental Saltwater Intrusion Drives Rapid Soil Elevation and Carbon Loss in Freshwater and Brackish Everglades Marshes. *Estuaries Coasts* **2019**, *42*, 1868–1881. [CrossRef]
20. National Academies of Sciences, Engineering, and Medicine. *Progress Toward Restoring the Everglades: The Seventh Biennial Review—2018*; National Academies Press: Cambridge, MA, USA, 2019.
21. Hardisky, M.; Gross, M.; Klemas, V. Remote sensing of coastal wetlands. *Bioscience* **1986**, *36*, 453–460. [CrossRef]
22. Ozesmi, S.L.; Bauer, M.E. Satellite remote sensing of wetlands. *Wetl. Ecol. Manag.* **2002**, *10*, 381–402. [CrossRef]
23. Klemas, V. Remote sensing techniques for studying coastal ecosystems: An overview. *J. Coast. Res.* **2011**, *27*, 2–17.
24. Rundquist, D.C.; Narumalani, S.; Narayanan, R.M. A review of wetlands remote sensing and defining new considerations. *Remote Sens. Rev.* **2001**, *20*, 207–226. [CrossRef]
25. Adam, E.; Mutanga, O.; Rugege, D. Multispectral and hyperspectral remote sensing for identification and mapping of wetland vegetation: A review. *Wetl. Ecol. Manag.* **2010**, *18*, 281–296. [CrossRef]
26. Moffett, K.B.; Nardin, W.; Silvestri, S.; Wang, C.; Temmerman, S. Multiple stable states and catastrophic shifts in coastal wetlands: Progress, challenges, and opportunities in validating theory using remote sensing and other methods. *Remote Sens.* **2015**, *7*, 10184–10226. [CrossRef]
27. Guo, M.; Li, J.; Sheng, C.; Xu, J.; Wu, L. A review of wetland remote sensing. *Sensors* **2017**, *17*, 777. [CrossRef] [PubMed]
28. Mahdavi, S.; Salehi, B.; Granger, J.; Amani, M.; Brisco, B.; Huang, W. Remote sensing for wetland classification: A comprehensive review. *GIScience Remote Sens.* **2018**, *55*, 623–658. [CrossRef]
29. Belgiu, M.; Drăguţ, L. Random forest in remote sensing: A review of applications and future directions. *ISPRS J. Photogramm. Remote Sens.* **2016**, *114*, 24–31. [CrossRef]
30. Breiman, L. Random forests. *Mach. Learn.* **2001**, *45*, 5–32. [CrossRef]
31. Whiteside, T.G.; Bartolo, R.E. Mapping aquatic vegetation in a tropical wetland using high spatial resolution multispectral satellite imagery. *Remote Sens.* **2015**, *7*, 11664–11694. [CrossRef]
32. Franklin, S.E.; Ahmed, O.S. Object-based wetland characterization using radarsat-2 quad-polarimetric SAR data, landsat-8 OLI imagery, and airborne lidar-derived geomorphometric variables. *Photogramm. Eng. Remote Sens.* **2017**, *83*, 27–36. [CrossRef]
33. Mutanga, O.; Adam, E.; Cho, M.A. High density biomass estimation for wetland vegetation using WorldView-2 imagery and random forest regression algorithm. *Int. J. Appl. Earth Obs. Geoinf.* **2012**, *18*, 399–406. [CrossRef]
34. Wendelberger, K.S.; Gann, D.; Richards, J.H. Using Bi-seasonal worldview-2 multi-spectral data and supervised random forest classification to map coastal plant communities in Everglades National Park. *Sensors* **2018**, *18*, 829. [CrossRef] [PubMed]

35. Morgan, J.L.; Gergel, S.E.; Coops, N.C. Aerial photography: A rapidly evolving tool for ecological management. *BioScience* **2010**, *60*, 47–59. [CrossRef]
36. Work, E.A.; Gilmer, D.S. Utilization of satellite data for inventorying prairie ponds and lakes. *Photogramm. Eng. Remote Sens.* **1976**, *42*, 685–694.
37. Lyon, J.G.; Greene, R. Use of aerial photographs to measure the historical areal extent of Lake Erie coastal wetlands. *Photogramm. Eng. Remote Sens.* **1992**, *58*, 1355–1360.
38. Williams, D.C.; Lyon, J.G. Historical aerial photographs and a geographic information system (GIS) to determine effects of long-term water level fluctuations on wetlands along the St. Marys River, Michigan, USA. *Aquat. Bot.* **1997**, *58*, 363–378. [CrossRef]
39. Cserhalmi, D.; Nagy, J.; Kristóf, D.; Neidert, D. Changes in a wetland ecosystem: A vegetation reconstruction study based on historical panchromatic aerial photographs and succession patterns. *Folia Geobot.* **2011**, *46*, 351–371. [CrossRef]
40. Ballanti, L.; Byrd, K.B.; Woo, I.; Ellings, C. Remote sensing for wetland mapping and historical change detection at the Nisqually River Delta. *Sustainability* **2017**, *9*, 1919. [CrossRef]
41. Rapinel, S.; Clément, B.; Dufour, S.; Hubert-Moy, L. Fine-scale monitoring of long-term wetland loss using LiDAR data and historical aerial photographs: The example of the couesnon floodplain, France. *Wetlands* **2018**, *38*, 423–435. [CrossRef]
42. Lillesand, T.M.; Kiefer, R.W.; Chipman, J. *Remote Sensing and Image Interpretation*; John Willey & Sons. Inc.: Hoboken, NJ, USA, 1994.
43. Saura, S. Effects of minimum mapping unit on land cover data spatial configuration and composition. *Int. J. Remote Sens.* **2002**, *23*, 4853–4880. [CrossRef]
44. Knight, J.F.; Lunetta, R.S. An experimental assessment of minimum mapping unit size. *IEEE Trans. Geosci. Remote Sens.* **2003**, *41*, 2132–2134. [CrossRef]
45. Rutchey, K.; Godin, J. Determining an appropriate minimum mapping unit in vegetation mapping for ecosystem restoration: A case study from the Everglades, USA. *Landsc. Ecol.* **2009**, *24*, 1351–1362. [CrossRef]
46. Lodge, T.E. *The Everglades Handbook: Understanding the Ecosystem*; CRC Press: Boca Raton, FL, USA, 2016.
47. Yao, Q.; Liu, K.-B. Dynamics of marsh-mangrove ecotone since the mid-Holocene: A palynological study of mangrove encroachment and sea level rise in the Shark River Estuary, Florida. *PLoS ONE* **2017**, *12*, e0173670. [CrossRef] [PubMed]
48. Scholl, D.W. Recent sedimentary record in mangrove swamps and rise in sea level over the southwestern coast of Florida: Part 2. *Mar. Geol.* **1964**, *2*, 343–364. [CrossRef]
49. Smith, W.G. Sedimentary Environments and Environmental Change in the Peat-Forming Area of South Florida. Ph.D. Thesis, The Pennsylvania State University, State College, PA, USA, 1970.
50. Parkinson, R.W. Decelerating Holocene sea-level rise and its influence on Southwest Florida coastal evolution; a transgressive/regressive stratigraphy. *J. Sediment. Res.* **1989**, *59*, 960–972.
51. Kaplan, S.W. Peat Records of Late Holocene Climate and Sea Level Change in South Florida. Ph.D. Thesis, University of Wisconsin–Madison, Madison, WI, USA, 2004.
52. Volety, A.K.; Savarese, M.; Hoye, B.; Loh, A.N. *Landscape Pattern: Present and Past Distribution of Oysters in South Florida Coastal Complex (Whitewater Bay/Oyster Bay/Shark to Robert's Rivers)*; South Florida Water Management District Final Technical Report; Florida Gulf Coast University: West Palm Beach, FL, USA, 2009.
53. Davis, S.; Ogden, J.C. *Everglades: The Ecosystem and Its Restoration*; CRC Press: Boca Raton, FL, USA, 1994.
54. Childers, D.L.; Gaiser, E.; Ogden, L.A. *The Coastal Everglades: The Dynamics of Social-Ecological Transformation in the South Florida Landscape*; Oxford University Press: Oxford, UK, 2019.
55. McVoy, C.; Said, W.P.; Obeysekera, J.; VanArman, J.A.; Dreschel, T.W. *Landscapes and Hydrology of the Predrainage Everglades*; University Press of Florida Gainesville: Gainesville, FL, USA, 2011.
56. Aich, S.; McVoy, C.W.; Dreschel, T.W.; Santamaria, F. Estimating soil subsidence and carbon loss in the Everglades Agricultural Area, Florida using geospatial techniques. *Agric. Ecosyst. Environ.* **2013**, *171*, 124–133. [CrossRef]
57. Hohner, S.M.; Dreschel, T.W. Everglades peats: Using historical and recent data to estimate predrainage and current volumes, masses and carbon contents. *Mires Peat.* **2015**, *16*, 1–15.
58. Foster, A. *Historic Aerial Photography of the Greater Everglades Archive and Geodatabase Development*; USGS Publications Warehouse: Restond, VA, USA, 2004; pp. 2327–6932.
59. Hijmans, R.J.; Van Etten, J.; Cheng, J.; Mattiuzzi, M.; Sumner, M.; Greenberg, J.A.; Lamigueiro, O.P.; Bevan, A.; Racine, E.B.; Shortridge, A. Raster: Geographic Data Analysis and Modeling. R Package Version 2.8-4. 2015. Available online: https://CRAN.R-project.org/package=raster (accessed on 19 June 2022).
60. Kuhn, M.; Wing, J.; Weston, S.; Williams, A.; Keefer, C.; Engelhardt, A.; Cooper, T.; Mayer, Z.; Kenkel, B.; Team, R.C. Caret: Classification and Regression Training. R Package Version 6.0-80. 2020. Available online: https://CRAN.R-project.org/package=caret (accessed on 19 June 2022).
61. Jordan, C.F. Derivation of leaf-area index from quality of light on the forest floor. *Ecology* **1969**, *50*, 663–666. [CrossRef]
62. Rousel, J.; Haas, R.; Schell, J.; Deering, D. Monitoring Vegetation Systems in the Great Plains with ERTS. In Proceedings of the Third Earth Resources Technology Satellite—1 Symposium, NASA SP-351, Washington, DC, USA, 10–14 December 1973; pp. 309–317.

63. Barnes, E.; Clarke, T.; Richards, S.; Colaizzi, P.; Haberland, J.; Kostrzewski, M.; Waller, P.; Choi, C.; Riley, E.; Thompson, T. Coincident detection of crop water stress, nitrogen status and canopy density using ground based multispectral data. In Proceedings of the Fifth International Conference on Precision Agriculture, Bloomington, MN, USA, 16–19 July 2000; p. 6.
64. McFeeters, S.K. The use of the Normalized Difference Water Index (NDWI) in the delineation of open water features. *Int. J. Remote Sens.* **1996**, *17*, 1425–1432. [CrossRef]
65. Gitelson, A.A.; Kaufman, Y.J.; Merzlyak, M.N. Use of a green channel in remote sensing of global vegetation from EOS-MODIS. *Remote Sens. Environ.* **1996**, *58*, 289–298. [CrossRef]
66. Huete, A.R. A soil-adjusted vegetation index (SAVI). *Remote Sens. Environ.* **1988**, *25*, 295–309. [CrossRef]
67. Jiang, Z.; Huete, A.R.; Didan, K.; Miura, T. Development of a two-band enhanced vegetation index without a blue band. *Remote Sens. Environ.* **2008**, *112*, 3833–3845. [CrossRef]
68. Serra, J. Introduction to mathematical morphology. *Comput. Vis. Graph. Image Processing* **1986**, *35*, 283–305. [CrossRef]
69. Heijmans, H.J. Mathematical morphology: A modern approach in image processing based on algebra and geometry. *SIAM Rev.* **1995**, *37*, 1–36. [CrossRef]
70. Soille, P.; Pesaresi, M. Advances in mathematical morphology applied to geoscience and remote sensing. *IEEE Trans. Geosci. Remote Sens.* **2002**, *40*, 2042–2055. [CrossRef]
71. R Core Team. *R: A Language and Environment for Statistical Computing*; R Foundation for Statistical Computing: Vienna, Austria, 2022.
72. Jensen, J.R. *Introductory Digital Image Processing: A Remote Sensing Perspective*; Prentice-Hall Inc.: Hoboken, NJ, USA, 1996.
73. Tillé, Y.; Matei, A.; Sampling: Survey Sampling. R Package Version 2.8. 2012. Available online: https://CRAN.R-project.org/package=sampling (accessed on 19 June 2022).
74. Olofsson, P.; Foody, G.M.; Herold, M.; Stehman, S.V.; Woodcock, C.E.; Wulder, M.A. Good practices for estimating area and assessing accuracy of land change. *Remote Sens. Environ.* **2014**, *148*, 42–57. [CrossRef]
75. McCarthy, M.J.; Jessen, B.; Barry, M.J.; Figueroa, M.; McIntosh, J.; Murray, T.; Schmid, J.; Muller-Karger, F.E. Automated high-resolution time series mapping of mangrove forests damaged by hurricane Irma in Southwest Florida. *Remote Sens.* **2020**, *12*, 1740. [CrossRef]
76. Wood, E.M.; Pidgeon, A.M.; Radeloff, V.C.; Keuler, N.S. Image texture as a remotely sensed measure of vegetation structure. *Remote Sens. Environ.* **2012**, *121*, 516–526. [CrossRef]
77. Hudak, A.T.; Wessman, C.A. Textural analysis of historical aerial photography to characterize woody plant encroachment in South African savanna. *Remote Sens. Environ.* **1998**, *66*, 317–330. [CrossRef]
78. Caridade, C.; Marçal, A.R.; Mendonça, T. The use of texture for image classification of black & white air photographs. *Int. J. Remote Sens.* **2008**, *29*, 593–607.
79. Biskup, B.; Scharr, H.; Schurr, U.; Rascher, U. A stereo imaging system for measuring structural parameters of plant canopies. *Plant Cell Environ.* **2007**, *30*, 1299–1308. [CrossRef]
80. U.S. Army Corps of Engineers. *Comprehensive Everglades Restoration Plan: Picayune Strand Restoration (Formally the South Golden Gate Estates Ecosystem Restoration)*; United States Army Corps of Engineers: Washington, DC, USA, 2004; p. 488.
81. Sklar, F.H.; Meeder, J.F.; Troxler, T.G.; Dreschel, T.; Davis, S.E.; Ruiz, P.L. The Everglades: At the Forefront of Transition. In *Coasts and Estuaries*; Elsevier: Amsterdam, The Netherlands, 2019; pp. 277–292.
82. DeLaune, R.D.; Nyman, J.A.; Patrick Jr, W. Peat collapse, ponding and wetland loss in a rapidly submerging coastal marsh. *J. Coast. Res.* **1994**, *4*, 1021–1030.
83. Wilson, B.J.; Servais, S.; Mazzei, V.; Kominoski, J.S.; Hu, M.; Davis, S.E.; Gaiser, E.; Sklar, F.; Bauman, L.; Kelly, S. Salinity pulses interact with seasonal dry-down to increase ecosystem carbon loss in marshes of the Florida Everglades. *Ecol. Appl.* **2018**, *28*, 2092–2108. [CrossRef] [PubMed]
84. Solohin, E.; Widney, S.E.; Craft, C.B. Declines in plant productivity drive loss of soil elevation in a tidal freshwater marsh exposed to saltwater intrusion. *Ecology* **2020**, *101*, e03148. [CrossRef] [PubMed]
85. Cahoon, D.R.; Hensel, P.; Rybczyk, J.; McKee, K.L.; Proffitt, C.E.; Perez, B.C. Mass tree mortality leads to mangrove peat collapse at Bay Islands, Honduras after Hurricane Mitch. *J. Ecol.* **2003**, *91*, 1093–1105. [CrossRef]
86. Day, J.W.; Kemp, G.P.; Reed, D.J.; Cahoon, D.R.; Boumans, R.M.; Suhayda, J.M.; Gambrell, R. Vegetation death and rapid loss of surface elevation in two contrasting Mississippi delta salt marshes: The role of sedimentation, autocompaction and sea-level rise. *Ecol. Eng.* **2011**, *37*, 229–240. [CrossRef]
87. Schepers, L.; Brennand, P.; Kirwan, M.L.; Guntenspergen, G.R.; Temmerman, S. Coastal Marsh Degradation Into Ponds Induces Irreversible Elevation Loss Relative to Sea Level in a Microtidal System. *Geophys. Res. Lett.* **2020**, *47*, e2020GL089121. [CrossRef]
88. Wang, C.; Schepers, L.; Kirwan, M.L.; Belluco, E.; D'Alpaos, A.; Wang, Q.; Yin, S.; Temmerman, S. Different coastal marsh sites reflect similar topographic conditions under which bare patches and vegetation recovery occur. *Earth Surf. Dyn.* **2021**, *9*, 71–88. [CrossRef]
89. Parkinson, R.W.; Wdowinski, S. Accelerating sea-level rise and the fate of mangrove plant communities in South Florida, USA. *Geomorphology* **2022**, *412*, e108329. [CrossRef]
90. Schuerch, M.; Spencer, T.; Temmerman, S.; Kirwan, M.L.; Wolff, C.; Lincke, D.; McOwen, C.J.; Pickering, M.D.; Reef, R.; Vafeidis, A.T. Future response of global coastal wetlands to sea-level rise. *Nature* **2018**, *561*, 231–234. [CrossRef]